5-1-2018

Ultra-wideband Single Jurkat Human T-lymphocyte Cell Characterization, Dielectrophoresis, and Electroporation Using One Vector Network Analyzer

Xiaotian Du
Lehigh University, xid415@lehigh.edu

Ultra-wideband Single Jurkat Human T-lymphocyte Cell Characterization, Dielectrophoresis, and Electroporation Using One Vector Network Analyzer

By

Xiaotian Du

A Thesis

Presented to the Graduate and Research Committee

Of Lehigh University

In Candidacy for the Degree of

Master of Science

In

Electrical Engineering

Lehigh University

April 2018

Xiaotian Du's Thesis Signature Sheet

This thesis is accepted and approved in partial fulfillment of the requirements for a Master of Science.

_____

Date

_____

Prof. James C.M. Hwang, Thesis Advisor

Compound Semiconductor Technology Lab

Professor of Electrical Engineering

_____

Prof. Chengshan Xiao

Chair of Electrical and Computer Engineering Department

Acknowledgement

I would like to first thank my advisor Professor James C.M. Hwang. I first met Jim, as we all call him, during my third year as an undergraduate student at Fudan University in Shanghai, China. He hosted an interview there and very kindly offered an opportunity for me to visit Lehigh and work on a research project during that summer with sponsorship. That summer was not only the start of the work reported in this thesis, but also the start of some real research life for me, after which I made up my mind to join Jim's group to continue this research as a Ph.D. student after receiving my bachelor's from Fudan University. It is his encouragement and kind offer of a great research opportunity that have made me here today devoting myself to a real scientific research life.

With a materials science background, I met lots of difficulties when I boldly jumped into electrical engineering at first. However, Jim was very patient and tried all the ways he can to encourage me and help me. It was his instructions and constructive criticism that helped me walk out of the days when I felt so lost at the beginning of this Ph.D. Journey. Besides, his courses were very enlightening and helpful, from which we not only learned knowledge, but also, more importantly, how to learn.

This research project has never been an easy one, but fortunately Jim can always give good directions when I don't know where to go. After this master's thesis, the road ahead to continue pursuing my Ph.D. degree might be even harder than before. But I have full confidence and determination that I can and will complete this journey as I am already this far.

This work wouldn't have been accomplished without the help of all the co-workers in our group, Xiao Ma, Lei Li, Kuanchen Xiong, Xin Jin, Xiaopeng Wang, Mohammad Asadi, Prof. Xuanhong Cheng, and also those who were here working close with me but have left for their new life trip, Dr. Hang Li, Zhibo Cao, Dr. Vahid Gholizadeh, Dr. Yaqing Ning, and Dr. Xi Luo. Great thanks to them for the help not only in my research and academic study, but also the help in my life.

I would also like to thank my parents who are always supporting me and giving me helpful advice. Thanks to my aunt who is the only relative I have in the United States for caring about me so much.

Table of Contents

Acknowledgement……iii

List of Figures……v

List of Tables……vii

Abstract……1

1. Introduction ……3

    1.1. Broadband Electrical Biosensing……3

    1.2. Challenges and Motivations……4

    1.3. Experimental Setup……6

2. Dielectrophoresis……10

    2.1. Theory of Dielectrophoresis……10

    2.2. Detrapping Experiment Design ……13

    2.3. Validation of Clausius-Mossotti Function ……14

    2.4. Summary……17

3. Ultra-wideband Single-Cell Characterization……18

    3.1. Experimental Protocol……18

    3.2. Two Configurations……20

    3.3 Background Drift Study……26

    3.4 Summary……28

4. Electroporation……29

    4.1. Theory……29

    4.2. Experimental Results……30

    4.3 Summary……30

5. Conclusions……..32

References……33

Vita……38

List of Figures

Figure 1: Schematic illustration of broadband dispersion of the dielectric properties of a biological cell showing transitions between different polarization mechanisms at different frequency ranges and length scales. ……4

Figure 2: Photograph of experimental setup with homemade probe station on inverted fluorescence microscope……6

Figure 3: 3 Schematic DUT with CPW between PDMS cover and quartz substrate……..7

Figure 4: Micrograph of a live Jurkat cell trapped in series CPW gap. Lateral dark bands are CPW electrodes. Vertical lines are microfluidic channel walls……..8

Figure 5 Micrograph of a single live Jurkat human T-lymphocyte cell in the culture media solution under an optical microscope……..9

Figure 6 Calculated frequency dependence of the real part of the Clausius-Mossotti function for a Jurkat cell suspended in sucrose solution……12

Figure 7: Micrographs of the same Jurkat cell (a) trapped by a pDEP signal at 10 MHz and (b) detrapped by an nDEP signal at 55 kHz. Horizontal lines intersecting lower cell edges quantify cell displacement……13

Figure 8: Cell displacement trajectory vs. DEP frequency at kHz range measured on sixteen different cells trapped and detrapped in sixteen single-cell DEP experiments……15

Figure 9: Cell displacement trajectory vs. DEP frequency at MHZ range measured on eight different cells trapped and detrapped in eight single-cell DEP experiments……16

Figure 10: Micrograph of different configurations of CPW under the optical microscope. The darker area is the microfluidic channel shaped by SU8 layer……19

Figure 11: Micrograph of single Jurkat cell trapped in the series gap……21

Figure 12: Micrograph of single Jurkat cell trapped in the shunt gap……21

Figure 13: Measured UWB insertion and return losses on a CPW with a series gap under air (red), air + SU8 (yellow), air + SU8 + PDMS (blue), and air + SU8 + PDMS + sucrose solution (green), respectively. Incident power = −18 dBm……22

Figure 14: Measured UWB insertion and return losses on a CPW with a shunt gap under air (red), air + SU8 (yellow), air + SU8 + PDMS (blue), and air + SU8 + PDMS + sucrose solution (green), respectively. Incident power = −18 dBm……24

Figure 15: Measured changes in (a) insertion loss and (b) return loss with a Jurkat cell trapped in series configuration. The experiment was repeated on four different cells……..25
Figure 16: Measured changes in (a) insertion loss and (b) return loss with a Jurkat cell trapped in shunt configuration. The experiment was repeated on three different cells……..26

Figure 17: Long-term drift of return and insertion losses at 9 GHz of a CPW with its series trap filled with sucrose solution…..27
Figure 18: Long-term drift of return and insertion losses at 9 GHz of a CPW with its shunt trap filled with sucrose solution……28
Figure 19: Micrographs of a Jurkat cell (a) trapped, (b) porated, and (c) detrapped in series configuration, with poration confirmed by red dye of propidium iodide. ……30

List of Tables

Table I: Permittivity and Thickness of Cell Compartments and Media ……..10

Table II: VNA Settings for Different Functions……..22

Abstract

For the first time, single-cell trapping, characterization, electroporation, and de-trapping were demonstrated by conveniently programming the frequency and power of the same ultra-wideband vector network analyzer (VNA) to perform the different functions across its bandwidth of 9 kHz–9 GHz. On one hand, trapping of a live biological cell was accomplished by applying to a coplanar waveguide (CPW) through the VNA a continuous wave (CW) signal of 3 dBm and 5 MHz, corresponding to attractive dielectrophoresis. On the other hand, detrapping of a live biological cell was also accomplished to complete a better control of the cell in microfluidics using electromagnetic method, after both the lower and the higher crossover frequencies of Clausius-Mossotti function were carefully studied. A detrapping experiment was designed to validate the CM function, which demonstrated that the lower and the higher crossover frequencies were around 60 kHz and 300 MHz, respectively, from positive force to negative force in single-cell dielectrophoresis predicted by the Clausius-Mossotti function theoretical calculation, despite the highly nonuniform electric field distribution between small and narrowly spaced electrodes, which was greatly disturbed by the cell. The validation was based on live Jurkat human T-lymphocyte cells that were resuspended in isotonic sucrose solution, and should be further tested on different cells in their culture media. With further validation, the Clausius-Mossotti function can be used to help optimize the dielectrophoresis configuration and algorithm for more complicated cell manipulation. After a cell is trapped on the CPW, the VNA was switched to 9 dBm and 100 kHz for electroporation. Before and after electroporation, the cell could be characterized from 9 kHz to 9 GHz by setting the VNA at −18 dBm to assess the effect of electroporation. This breakthrough not only greatly improves the accuracy and efficiency of

electrical cell characterization, but also can enable its throughput to approach that of optical cytometers in the future.

Chapter 1: Introduction

1.1 Broadband Electrical Biosensing

Compared with traditional chemical or optical detection, electrical biosensors present general advantages such as being compact, label-free, harmless to the cell, easy to automate, and inexpensive to manufacture. Electrical sensing of tissues and cells have been explored for more than a century, yet is mostly narrowband between kilohertz and megahertz frequencies with far-apart electrodes. The best example, the Coulter counter, has been widely adopted for clinical blood cell counts for more than 50 years, which operates in a label-free and high-throughput fashion. However, it uses one or several distinct frequencies in the kilohertz to low megahertz range and information obtained is mostly limited to cell size and membrane capacitance, because at such low frequencies the cell membrane appearing as an insulator to shield intra-cellular compartments. Advanced nano-electrodes that penetrate into cells have been reported to reveal properties of intra-cellular organelles, [1][2][3] but are invasive and difficult to standardize or scale up. Our recent research demonstrates that intra-cellular dielectric properties can be obtained through whole-cell electrical sensing within an ultra-wideband from kilohertz up to the gigahertz range, so that the cell membrane becomes transparent to the electric field and intra-cellular dielectric properties can be extracted with high accuracy and repeatability.[4][5]

This is mainly because the cell membrane and intra-cellular compartments have distinct dielectric properties, so that the membrane capacitance dominates the cell impedance in the kilohertz-to-megahertz range, but becomes negligible at higher frequencies, as illustrated in Fig.

1. By contrast, under an optical microscope most intra-cellular compartments appear transparent and show little contrast without labeling. Additionally, with closely spaced electrodes in near-field interaction with a cell, subcellular spatial resolution is possible despite the long wavelength at microwave frequencies or below. The strong absorption of microwave signals by aqueous solutions and water-rich cells indicates high sensitivity instead of hindrance for near-field sensing.

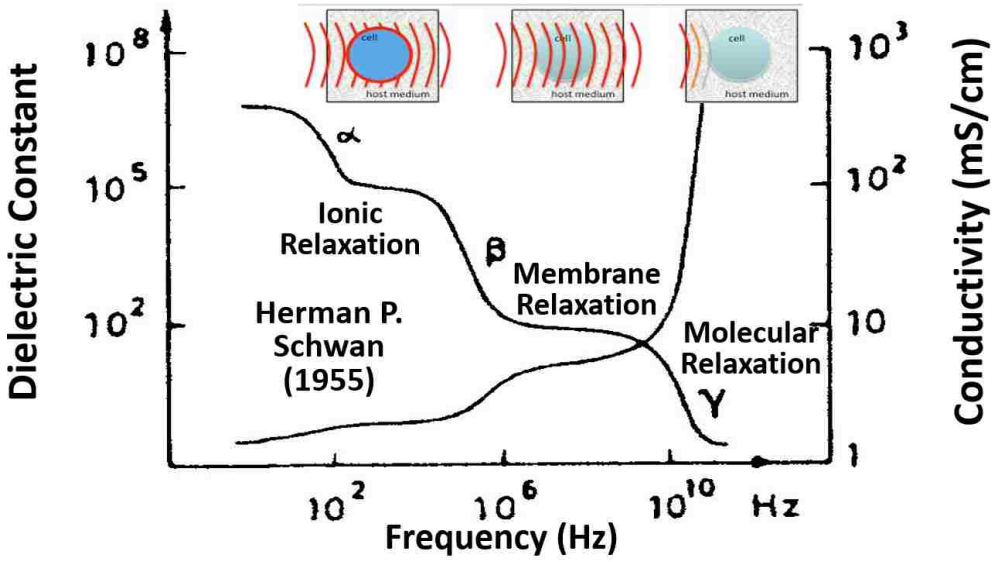

Fig. 1 Schematic illustration of broadband dispersion of the dielectric properties of a biological cell showing transitions between different polarization mechanisms at different frequency ranges and length scales.

1.2 Challenges and Motivations

Traditionally, impedance spectroscopy [6] or dielectric spectroscopy [7] has been performed at radio frequencies by using an impedance analyzer on a suspension of biological cells. Recently, the spectrum was extended to microwave frequencies by using a vector network analyzer (VNA)

on a single cell trapped alive either mechanically [8] or electrically [9]. However, most microwave VNAs have a lower cutoff on the order of 100 MHz, making it difficult to relate the recently obtained cell characteristics at microwave frequencies with the well-established cell characteristics at radio frequencies.

Unlike mechanical cell trapping, electrical cell trapping can be quickly turned on and off, allowing the small signal induced by a cell, on the order of 0.01 dB, to be accurately extracted amidst a drifting background [10]. Electrical cell trapping is usually performed by coupling the dielectrophoresis (DEP) signal, on the order of 10 MHz, from a function generator through a bias tee onto the microwave signal path of a VNA. This combination not only is cumbersome, but also limits the lower frequency of the VNA sweep regardless its bandwidth, and the upper frequency of the DEP signal which may be utilized to de-trap the cell. For example, for the present case of a Jurkat T-lymphocytes human cell suspended in isotonic sucrose solution, the DEP force switches from repulsive to attractive around 50 kHz and then from attractive to repulsive again around 1 GHz [11]. Obviously, 1 GHz is beyond the cutoff of most bias tees. Similarly, recent experiments have shown that electroporation of a cell membrane can be surprisingly effective at 10 MHz and higher [12], which is beyond the cutoff of most bias tees, too.

For the first time, we have overcome the low-frequency limit of most VNAs and high-frequency limit of most bias tees by using the same ultra-wideband (UWB) VNA with a bandwidth 9 kHz–9 GHz and without any bias tee. In particular, simply by programming the frequency and power of the VNA, we have successfully trapped, characterized, porated, recharacterized (to assess the poration effect), and de-trapped a cell. This breakthrough not only greatly improves the accuracy and efficiency of RF-microwave cell characterization, but also can enable its

throughput to approach that of optical cytometers in the future by programming the whole process with only one network analyzer under a constant flow.

1.3 Experimental Setup

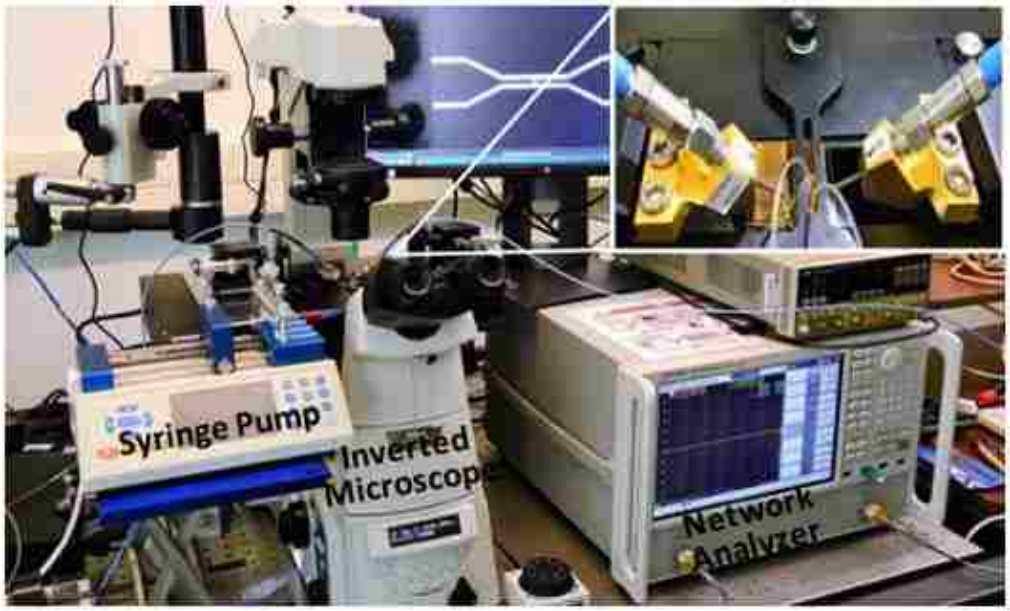

Fig. 2 Photograph of experimental setup with homemade probe station on inverted fluorescence microscope.

Fig. 2 shows the present setup contains a homemade microwave probe station which is on top of a Nikon Eclipse Ti-E inverted fluorescence microscope. A Keysight E5080A network analyzer with a pair of Cascade Microtech ACP40 GSG 100-µm pitched probes has been used to generate the specific signal depended on the functions. Fig.3 schematically demonstrates that the DUT is based on a gold coplanar waveguide (CPW) sandwiched between a quartz substrate and a polydimethylsiloxane (PDMS) cover. The PDMS cover is 8-mm long, 5-mm wide, 4-mm high.

The CPW is patterned in 0.5-µm-thick gold on 500-µm-thick quartz with a center electrode mostly 40-µm wide and 10 µm from the two 100-µm-wide ground electrodes on both sides. The center electrode is tapered down to 10 µm with a 10-µm-wide gap in the middle. This 10 µm × 10 µm gap is where the field gradient is maximized and is used to trap a live Jurkat cell by pDEP as shown in Fig. 4. An improvement of our current design is that a 20-µm thick SU-8 layer has been fabricated between the 0.5-µm-thick gold CPW layer and PDMS cover to better seal the solution leakage, thus enhancing the stability of the measurements. The microfluidic channel intersected perpendicularly to the CPW is also patterned by the SU8 layer instead of being etched into the PDMS cover as before. [4][5] The patterning strategy using SU-8 will also provide us with easier approach to pattern the channel in the shape as wanted.

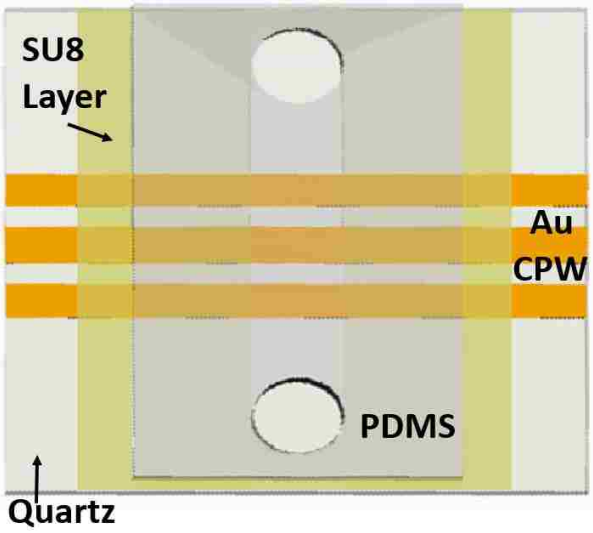

Fig. 3 Schematic DUT with CPW between PDMS cover and quartz substrate.

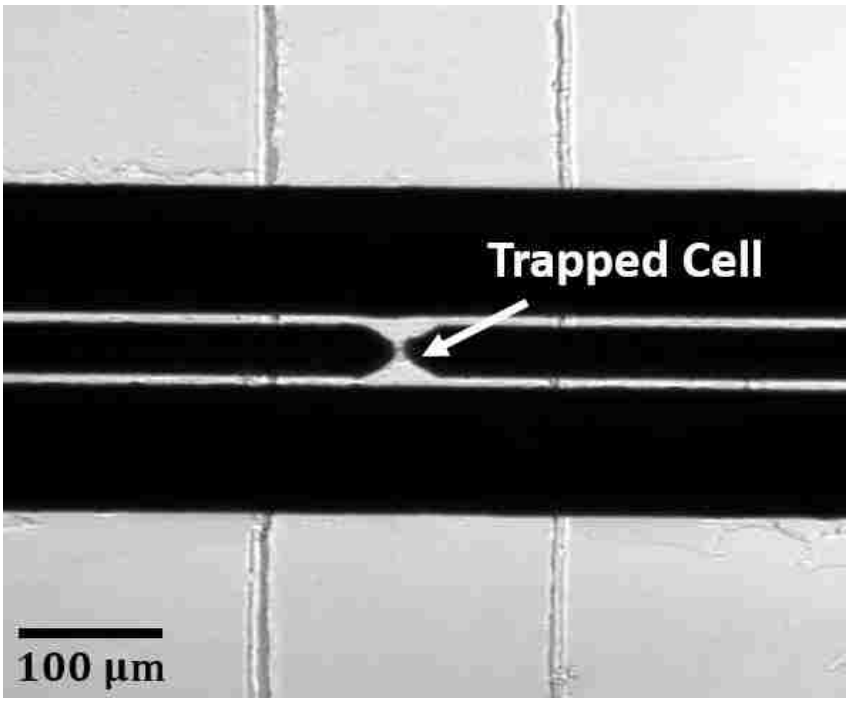

Fig. 4 Micrograph of a live Jurkat cell trapped in series CPW gap. Lateral dark bands are CPW electrodes. Vertical lines are microfluidic channel walls.

For proof of concept, Jurkat cells were chosen for their simple structure, large diameter (~10 µm), and nonadherent nature, which is shown in Fig.5. Cells were cultured in Sigma-Aldrich RPMI 1640, 10% fetal bovine serum, 100 units/mℓ penicillin, and 100 µg/mℓ streptomycin in a 37°C, 5% CO2 incubator. Cells were twice washed before resuspension in an isotonic solution with 8.5% sucrose and 0.3% dextrose. The resuspended cells were injected through the microfluidic channel at a rate of 0.1µℓ/min. Cell viability was tested in a separate experiment with trypan blue staining, which showed more than half of cells were alive after 10 h [10].

Fig. 5 Micrograph of a single live Jurkat human T-lymphocyte cell in the culture media solution under an optical microscope.

Chapter 2: Dielectrophoresis

2.1 Theory of Dielectrophoresis

Dielectrophoresis (DEP) has been widely used to sort or otherwise manipulate biological cells. DEP was first observed on small plastic particles that were neutral, spherical, homogenous, and suspended in a conductive solution. [13] When the particles were polarized by an applied electric field, they would move if the field was not uniform. The time-averaged moving force F can be related to the field gradient E (root-mean-square-averaged across the particle) by the real part of the Clausius-Mossotti (C-M) function K(ω), where ω is the angular frequency [14]. Thus,

$$F = 2\pi\varepsilon_S r^3 \,\mathrm{Re}\left[K(\omega)\right]\nabla\left|E\right|^2 \qquad (1)$$

where ε_S is the real part of the solution permittivity, and r is the particle radius. As illustrated in Fig. 6, depending on the frequency, the real part of K(ω) can be positive or negative, so that the particle can be moved toward where the field gradient is at the maximum or minimum, which is referred to as pDEP or nDEP.

TABLE I
PERMITTIVITY AND THICKNESS OF CELL COMPARTMENTS AND MEDIA SOLUTIONS

Compartment	$\varepsilon'(\varepsilon_0)$	σ (S/m)	d (μm)	Ref.
Cytoplasm	67.0	0.3	8	[4]
Membrane	11.7	1.10×10^{-7}	0.01	[5]
Sucrose	76.0	0.0027	2	[6]
Quartz	3.8	0	∞	[7]

Recently, we took advantage of the frequency dependence of DEP to trap a live Jurkat human T-lymphocyte cell by pDEP for electroporation and impedance spectroscopy, then to detrap it by nDEP so that the same trap can be quickly reused for another cell [15]. For the first time, pDEP, nDEP, electroporation, and impedance spectroscopy were all expediently accomplished by switching the frequency and power of the same ultra-wideband (UWB) vector network analyzer. In addition to convenience, the setup also offers an opportunity to study the trapping/detrapping dynamics of a cell individually, and to check whether or not the C-M function is valid for single-cell DEP. Note that single-cell DEP typically uses microelectrodes with size and spacing comparable to the cell radius, so that the resulted electric field is highly nonuniform and is greatly disturbed by the presence of a cell. However, the C-M function was developed for conventional DEP, which typically uses relatively large electrodes that are spaced far apart to accommodate a suspension of thousands of cells. In this case, the electric field distribution was assumed to be unperturbed by a cell.

This work reports, for the first time, that the cross-over frequency around 60 kHz from nDEP to pDEP in single-cell DEP is in general agreement with that predicted by the C-M function. Encouraged by these initial results, the cross-over frequency around 800 MHz from pDEP back to nDEP have also been validated experimentally within a reasonable difference from the calculated result. Note that frequencies as high as 800 MHz is beyond most DEP setups, whereas the present UWB setup is capable of well-controlled waveforms from 9 kHz to 9 GHz.

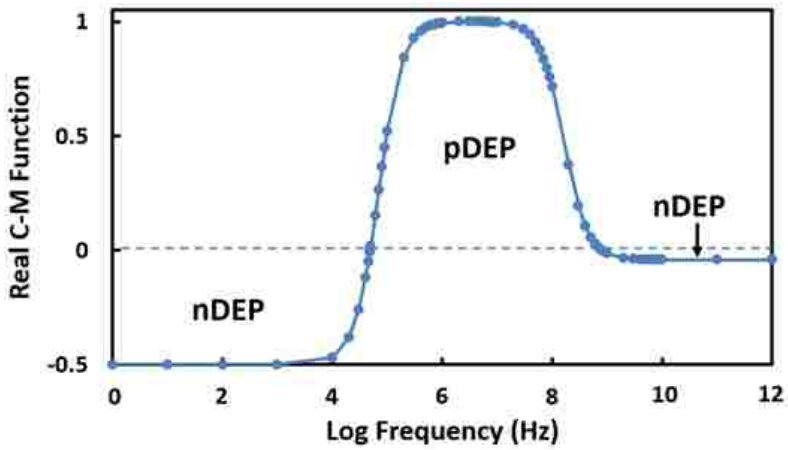

Fig. 6 Calculated frequency dependence of the real part of the Clausius-Mossotti function for a Jurkat cell suspended in sucrose solution.

Using a simple single-shell model of a spherical cell membrane enclosing a homogenous cytoplasm, the C-M function can be expresses as (2)

$$K(\omega) = -\frac{\omega^2(\tau_L\tau_M - \tau_C\tau_M') + j\omega(\tau_M' - \tau_L - \tau_M) - 1}{\omega^2(\tau_C\tau_M' + 2\tau_L\tau_M) - j\omega(\tau_M' + 2\tau_L + \tau_M) - 2} \quad (2)$$

where $\tau_L = \varepsilon_L/\sigma_L$, $\tau_M = rc_M/\sigma_C$, $\tau'_M = rc_M/\sigma_L$, $\tau_C = \varepsilon_C/\sigma_C$, σ_L is the solution conductivity, c_M is the membrane capacitance per unit area, σ_C is the cytoplasm conductivity, and ε_C is the real part of the cytoplasm permittivity. Using previously established parameter values for a Jurkat cell as the conductivity of the media and the cytoplasm being 0.0027 S/m and 0.3 S/m, respectively [16], the real part of (2) was evaluated as shown in Fig. 6. It can be seen that the real K(ω) is negative at the low-frequency limit, turns positive around 50 kHz, and becomes negative again above 800

MHz. These calculations were based on the parameters listed in Table I [17] and were used to guide the single-cell DEP experiments described in the next section.

2.2 Detrapping Experiment Design

Jurkat cells were trapped singularly by a pDEP signal of 0 dBm and 10 MHz generated by the VNA. Proper trapping was verified through the microscope, before the flow was stopped to avoid dislodging the cell without the pDEP signal. Thereafter, the VNA was programmed to generate a test nDEP signal at 3 dBm while stepping from 100 kHz down by 5 kHz every 4.2 s. (Higher nDEP power was necessary because, according to Fig. 6, the low-frequency nDEP force is only approximately half of the pDEP force at the same field strength.) Meanwhile, micrographs were recorded in real time and post-processed by the Nikon AR Elements software to quantify the cell displacement at any given moment. Fig.7 illustrates that the displacement was measured by the shift of the bottom edge of the cell as indicated by the horizontal green lines before and after detrapping. This experiment was repeated sixteen times on sixteen different cells for the validation of the lower crossover frequency.

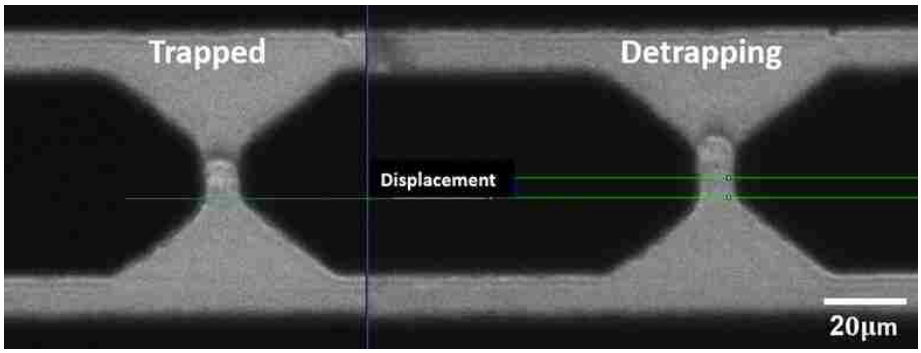

(a) (b)

Fig. 7 Micrographs of the same Jurkat cell (a) trapped by a pDEP signal at 10 MHz and (b) detrapped by an nDEP signal at 55 kHz. Horizontal lines intersecting lower cell edges quantify cell displacement.

2.3 Validation of Clausius-Mossotti Function

Now we talk about the validation of the lower crossover first, before we jump to the higher one. Fig. 8 traces the displacement of each cell with the horizontal scale converted from time to frequency, so that the intercept of each trajectory with the horizontal axis can be considered as the detrapping frequency. It can be seen that, once detrapped, a cell can move several micrometers in 4.2 s before the frequency is stepped lower. Thus, the coupling of time and frequency in the present experiment is not significant from the intercept point of view. The coupling is more significant after the cell is detrapped. However, the exact trajectory then is presently not of interest except to help visualize the intercept point. The trajectory also helps ensure the cell is completely detrapped, which is mostly the case except one outlier that turns back at 65 kHz before it is detrapped again at 50 kHz. Based on the sixteen cases shown in Fig. 8, the detrapping frequency, or the frequency DEP crosses from positive to negative, was determined to be 63 ± 11 kHz. Considering the heterogeneity of biological cells and the uncertainty in cell properties, this is reasonable agreement with that predicted by the C-M function and shown in Fig. 6 to be around 50 kHz. With the DEP frequency sweeping from the pDEP range down to the nDEP range in Fig. 6, the non-zero displacement happens at the crossover point and gets recorded in Fig. 8. The heating effect of the DEP signal is confirmed in a separated electroporation experiment [16], where the isotonic sucrose solution was

supplemented with 50 ml of 2'-7'-bis-(2-carboxy-ethyl)-5-(and-6)-carboxy-fluorescein, whose fluorescence intensity is sensitive to a temperature change of less than 1°C [18], and the fluorescence results demonstrated that the temperature change was negligible within the experiment time even applied by a much higher power of electroporation. Despite a well-matched experimental results predicted by CM function, the distributed effect caused by the cell with a similar size to the small electrode gap will be continuously studied by detailed simulations of the electric field distributions in the gap with a cell trapped in. The deviation of the crossover frequency of the sixteen cells may be also related to the size and shape variations of the cell, which needs further studies.

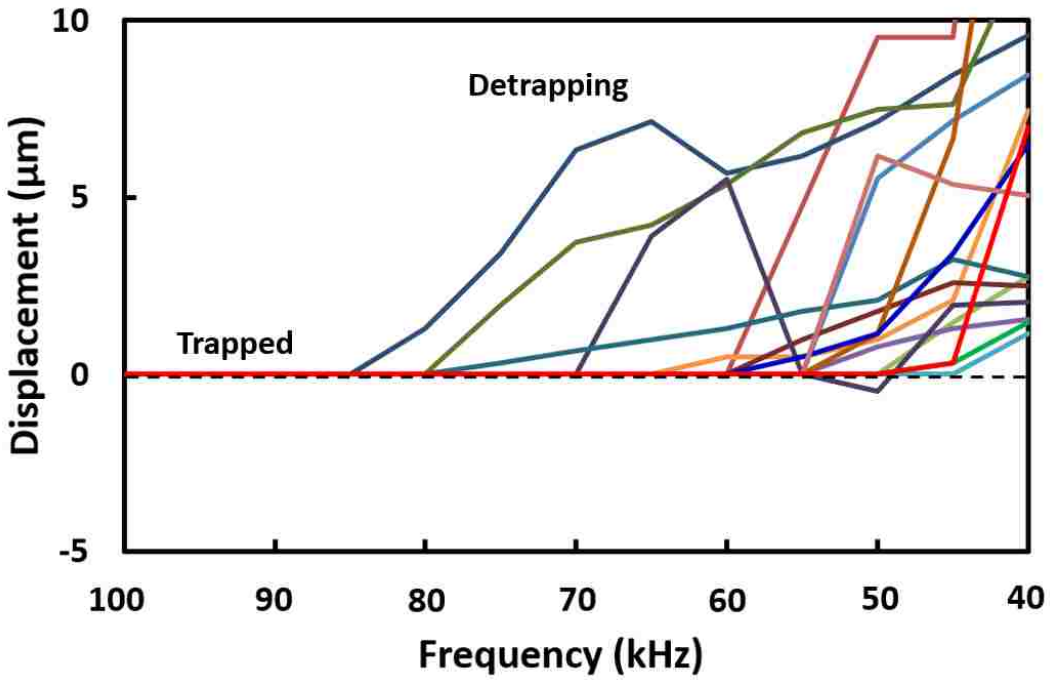

Fig. 8 Cell displacement trajectory vs. DEP frequency at kHz range measured on sixteen different cells trapped and detrapped in sixteen single-cell DEP experiments.

Using the same strategy, for the first time, the higher crossover frequency has also been validated, as is demonstrated in Fig. 9. This time, the cell was stably trapped with the signal of 5 MHz and 3 dBm, after which the VNA was controlled to sweep up to 1 GHz, with a frequency step and time interval being 50 MHz and 4s, respectively. As shown in Fig. 9, eight cells were measured and the displacements were recorded. We still focused on the frequency where first non-zero displacement happened. There three of them got detrapped at 250 MHz, one got detrapped at 300 MHz, and four of them got detrapped at 350 MHz. Therefore we draw a conclusion that the validation result for higher crossover frequency is 306 ± 50 MHz, which is in an acceptable range of agreement with the calculated result.

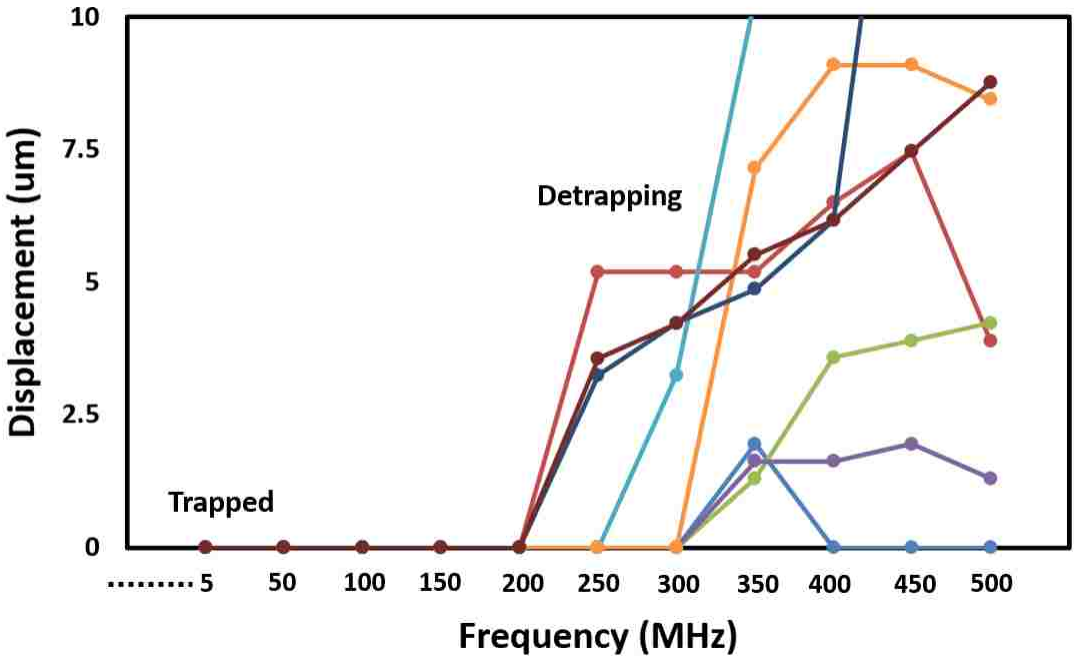

Fig. 9 Cell displacement trajectory vs. DEP frequency at MHZ range measured on eight different cells trapped and detrapped in eight single-cell DEP experiments.

For the difference between the calculation and the experiment, there are a few possible reasons to be discussed. First is that the conductivity of the solution may be different from the parameters used for calculation. Second is that the membrane capacitance dominates the cell impedance in the kilohertz-to-megahertz range, but becomes negligible at higher frequencies, and the intra-cellular structure may play an important role in the response to the DEP force. Therefore the calculation based on the single-shell Protoplast model may not work as well as for the lower crossover frequency. Notice that this validation of higher crossover frequency at GHz range can only be achieved with the network analyzer, as most of the functional generator is limited up to 10 MHz order of magnitude.

2.4 Summary

Dielectrophoresis, as a useful tool for manipulation of biological cells, has been used in CPW for trapping and detrapping purpose in our experiments. The breakthrough of utilization of DEP introduced in this chapter is that, for the first time, DEP signal is generated by a vector network analyzer with single-cell successfully trapped in the gap. What's more, both the lower and the higher crossover frequencies of the Clausius-Mossotti Function have been validated experimently and matched the calculated results very well. An effective trapping and detrapping manipulation is one of the most important part for improving the throughput as a future goal.

Chapter 3: Characterization

3.1 Experimental Protocol

After the network analyzer was well calibrated, the network analyzer was first acting as the trapping signal generator with the cells continuously flowing through the gap of transmission line along the microfluidic channel at a constant rate equal to 0.1 ul/min that is quite a slow rate suitable for trapping. Based on a large amount of experiments, the trapping frequency and power of the network analyzer was finally set to be 5 MHz and 3 dBm, respectively, which are efficient values for applying positive DEP (p-DEP), which has been carefully introduced in the last section, in the specific configurations of CPW shown in Fig 10. As the signal was triggered as *Continuous Sweep* on the trapping frequency, the cells would be efficiently trapped in between the ground line and the signal line once they passed by the gap very slowly. The moment the number of the trapped cells reached the wanted value, the pump was paused and also the power of trapping signal was decreased from 3 dBm to 0 dBm. Empirically, this value can significantly reduce the possibility of trapping more cells than wanted by effectively decreasing the intensity of p-DEP, meanwhile still being positive DEP force to keep the trapped cells remained in the gap. Normally, we will then wait for another two minutes to make sure the cells have been trapped stably. To this end, the trapping stage has been accomplished by the network analyzer.

Then the frequency and the power would be switched to the characterizing signal which was 9 kHz to 9 GHz sweeping range, and -18 dBm, respectively. The Ultra-wideband measurement would be accomplished by triggering a *Single Sweep* on the network analyzer, after which the data would be saved. Measurements for the same trapped cells were conducted for

three times to calculate the average for future data analysis, in order to decrease the possibility of incidental error. The average value was regarded as the representative value of cells signal.

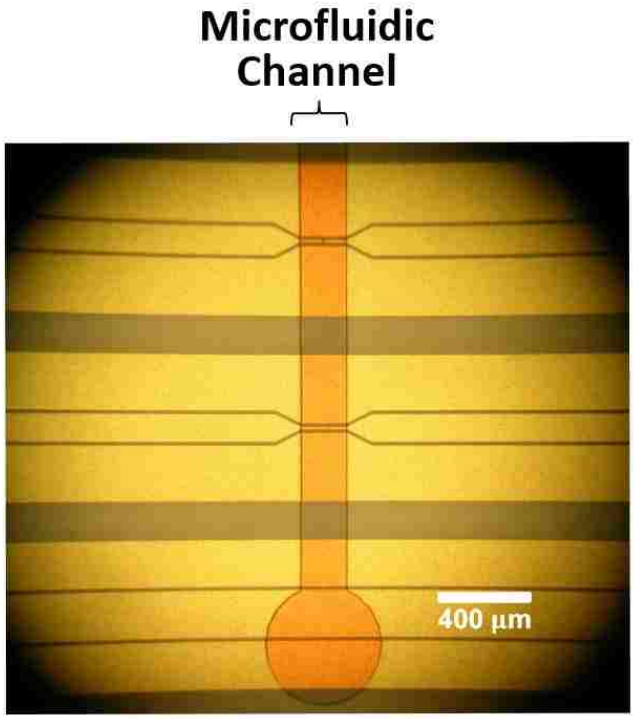

Fig. 10 Micrograph of different configurations of CPW under the optical microscope. The darker area is the microfluidic channel shaped by SU8 layer.

After the measurements of cells, the background signal was measured thus detrapping by the network analyzer was needed. The frequency and the power were then switched to 10 kHz and 3 dBm, respectively, to generate negative-DEP force (n-DEP) which would be applied towards the direction of pushing away the cells. The pump was then restarted and a flow rate of 0.5 um/min was set to help wash the cells away from the gap. Once the gap was clear, the syringe pump would be paused once again, and we would wait for another 5 minutes till the flow being

still again before the signal was switched back to characterizing signal which was 9 kHz to 9 GHz and -18 dBm, to measure the background for three times as well. The average value was calculated to be chosen as the background reference.

For proof of principle, Jurkat cells were chosen for their large diameter, simple structure, and non-adherent nature. The cells were cultured in Sigma-Aldrich's RPMI 1640 with 10% fetal bovine serum, 100 units/mL penicillin, and 100 μg/ml streptomycin under 37 °C and 5% CO2. The cultured cells were twice washed and re-suspended in 8.5% sucrose and 0.3% dextrose. Cell viability was verified in a separate experiment with Trypan Blue dye, which showed more than half of cells survived after 10 h. For the present label-free experiment, the cell suspension was injected through the microfluidic channel at approximately 0.1 μL/min as controlled by a syringe pump.

3.2 Two Configurations

CW signals from 9 kHz to 9 GHz was applied to the CPW by the same VNA, after the cell was stably trapped using DEP described in the last section. Measured on the well-defined and calibrated CPW, Fig. 11 and Fig.12, for which we call series configuration and shunt configuration, respectively, show two different configurations where the single-cell measurements were accomplished with well-behaved and spurious-free UWB insertion and return losses, even when the channel is filled with sucrose solution.

The background signal was carefully studied first as it is an essential part of the protocol. For series configuration, in Fig 13, it can be seen that the present test setup takes full advantage

of the > 100 dB dynamic range of the VNA. However, the difference with and without SU8 or PDMS is not discernable when plotted on such a large scale. Similarly, the difference with and without a cell trapped, on the order of 0.01 dB, is also not discernable on this scale. The sensitivity is within the reasonable range as shown in Fig.14.

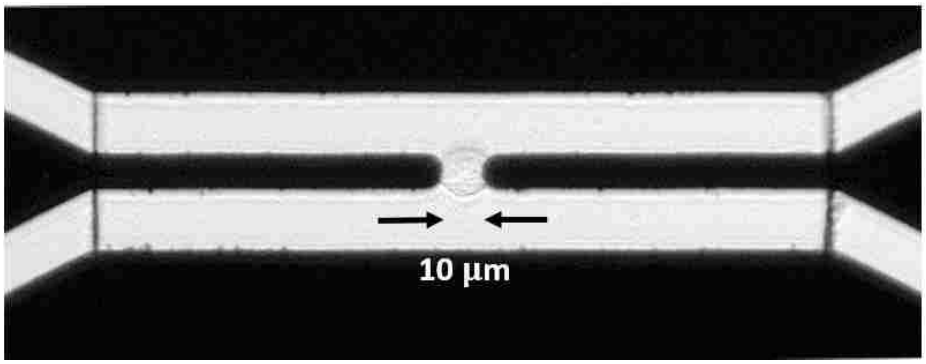

Fig. 11 Micrograph of single Jurkat cell trapped in the series gap.

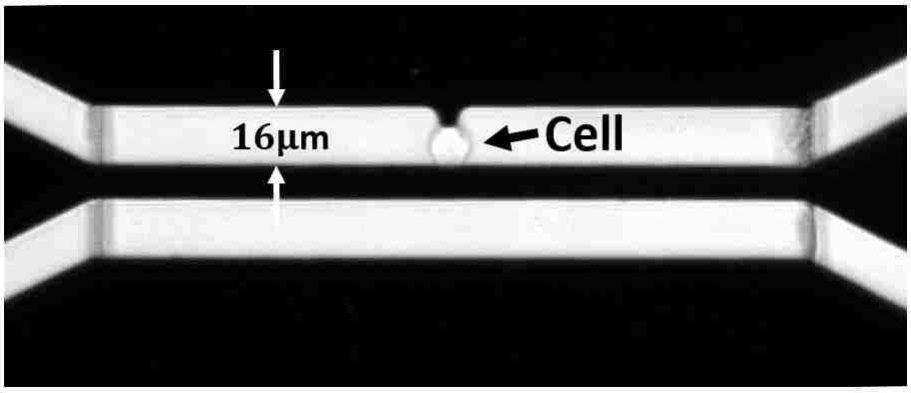

Fig. 12 Micrograph of single Jurkat cell trapped in the shunt gap.

As listed in Table II and shown in Fig. 11 and 12, once a cell was trapped by setting the VNA at 5 MHz and 3 dBm, it would remain in place under the slow flow. The VNA could then be

TABLE II
VNA SETTINGS FOR DIFFERENT FUNCTIONS

Function	Frequency	Power
Trapping	5 MHz	3 dBm
Characterizing	9 kHz–9 GHz	−18 dBm
Electroporation	100 kHz	9 dBm
De-trapping	10 kHz	3 dBm

set to sweep from 9 kHz to 9 GHz at −18 dBm for UWB characterization. Fig. 15 and Fig. 16 show the measured changes in insertion and return losses with a cell trapped in series and shunt configurations, respectively.

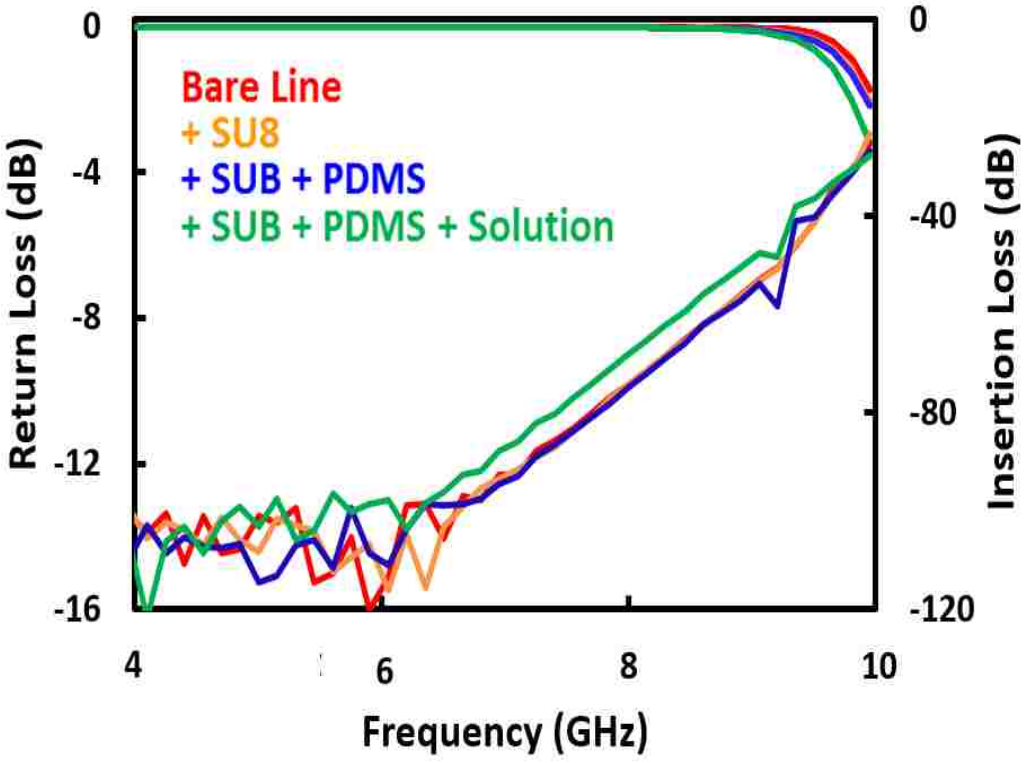

Fig. 13 Measured UWB insertion and return losses on a CPW with a series gap under air (red), air + SU8 (yellow), air + SU8 + PDMS (blue), and air + SU8 + PDMS + sucrose solution (green), respectively. Incident power = −18 dBm.

The experiment was repeated on four and three different cells trapped in series and shunt configurations, respectively. The results appear to be repeatable, despite the small signal magnitude and the natural cell variation. Although the signal magnitude varies greatly across the band, in general, the signal-to-noise ratio is better at microwave frequencies than at radio frequencies, which confirms the importance of extending cell characterization to the microwave range [19]. For example, the apparently > 10 dB signal around 1 MHz in Fig. 15 (a) is not particularly meaningful. This is because, with the insertion loss near the noise floor of −100 dB (Fig. 13), the change from −100 dB to −90 dB can be easily caused by calibration error. Changes in the phase of reflected and transmitted signals were also measured and recorded, although not shown. With a cell trapped, it can be electroporated by switching the VNA to 100 kHz and 9 dBm as listed in Table II.

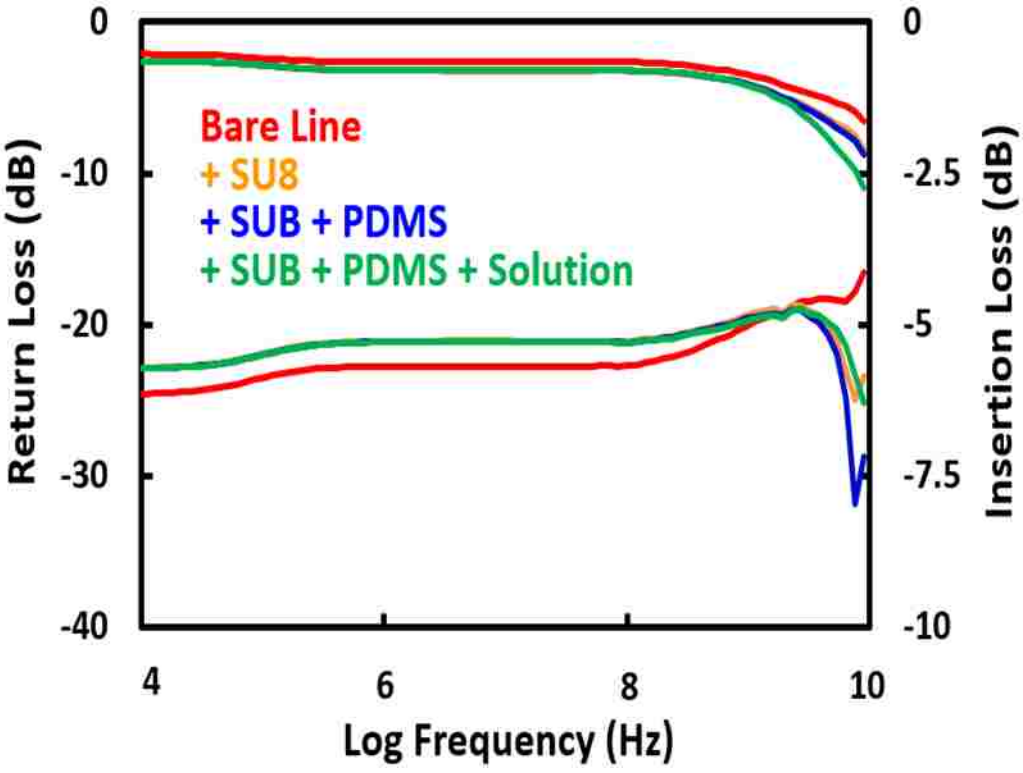

Fig. 14 Measured UWB insertion and return losses on a CPW with a shunt gap under air (red), air + SU8 (yellow), air + SU8 + PDMS (blue), and air + SU8 + PDMS + sucrose solution (green), respectively. Incident power = −18 dBm.

UWB characterization can then be conveniently performed before and after for correlation with changes in cell porosity, vitality and morphology, by using conventional fluorescent dyes [20]. Finally, the cell can be de-trapped by switching the VNA to 10 kHz at 3 dBM, so the sequence of trapping, characterization, poration, and detrapping can be repeated on the next available cell [21].

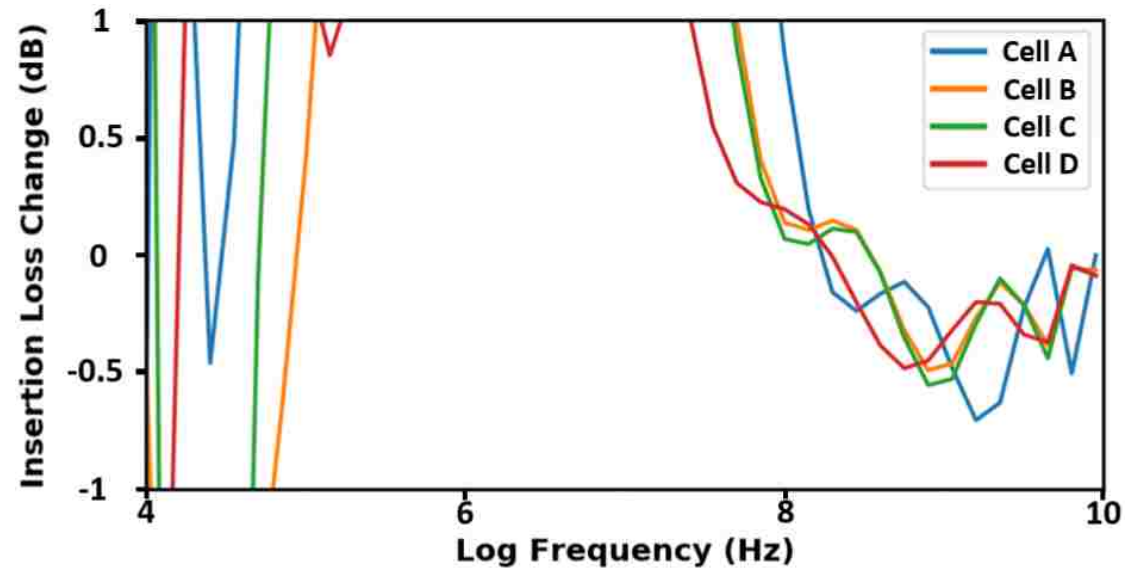

(a)

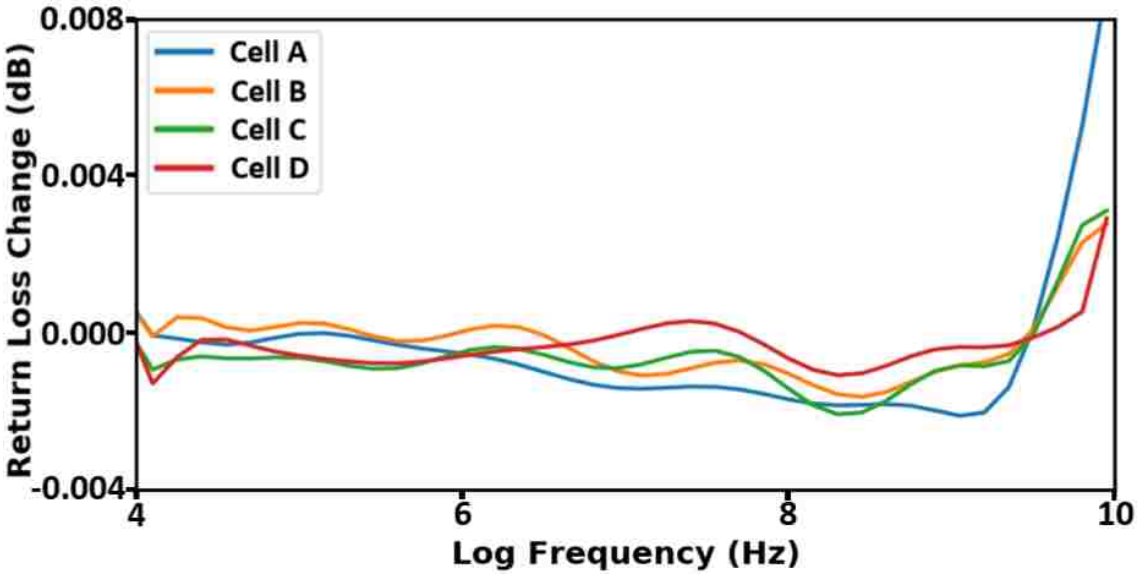

(b)

Fig. 15 Measured changes in (a) insertion loss and (b) return loss with a Jurkat cell trapped in series configuration. The experiment was repeated on four different cells.

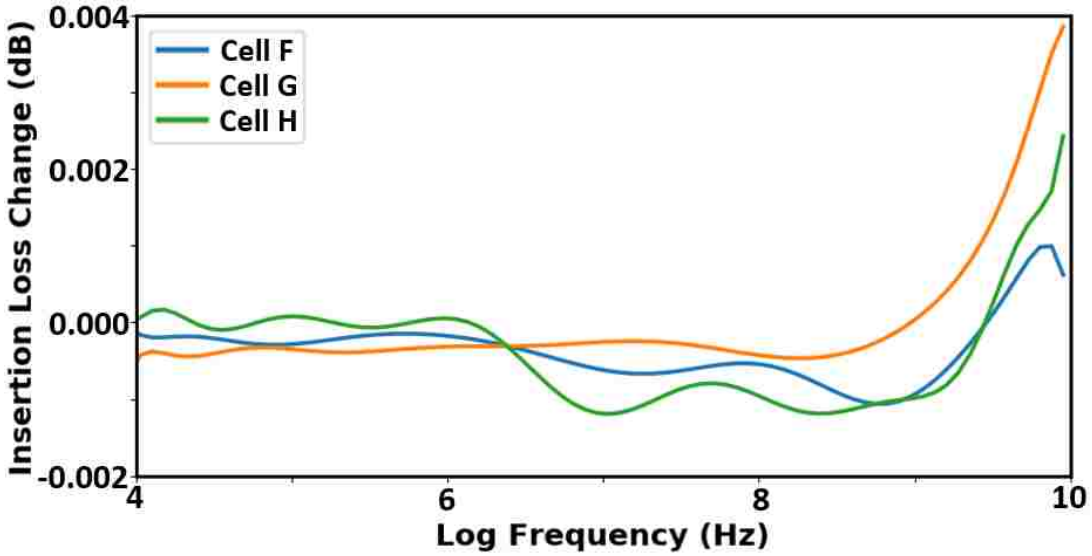

(a)

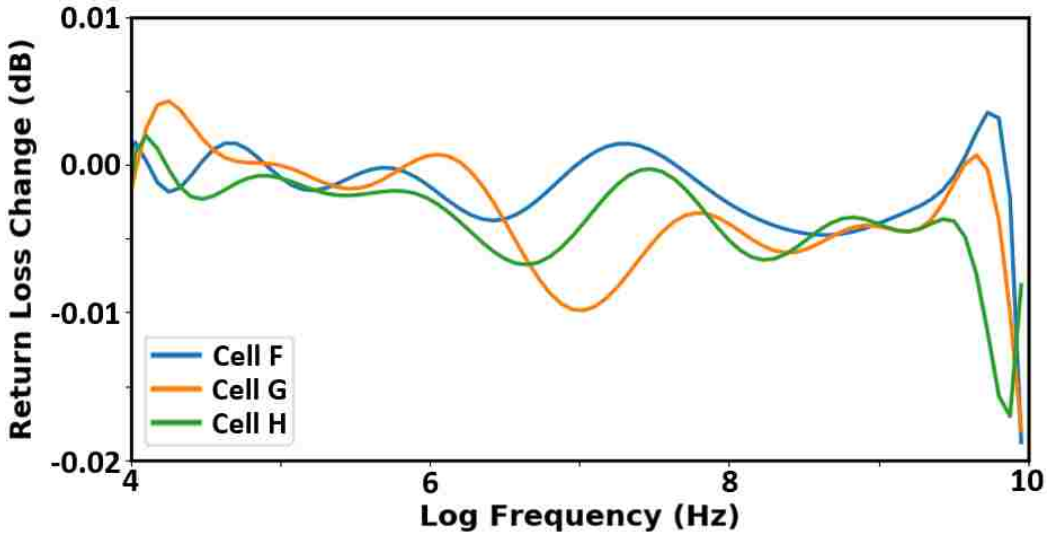

(b)

Fig. 16 Measured changes in (a) insertion loss and (b) return loss with a Jurkat cell trapped in shunt configuration. The experiment was repeated on three different cells.

3.3 Background Drift Study

By switching the DEP signal, the cell can be quickly trapped/detrapped and consecutive S-parameters measured in 1 min. This way, differences as small as 0.01 dB could be reproducibly measured amidst a slowly drifting background. Fig. 17 and Fig.18 show that despite care to

stabilize the setup calibration, the background signal of return loss and insertion loss without a cell typically drifted by approximately 0.001 dB/min, which satisfy the sensitivity of the results demonstrated in Fig 15 and 16. In fact, the present measurement setup is as sensitive as traditional interferometer measurements, except that it is performed in time domain instead of spatial domain. Note that traditional interferometer measurements are very difficult to be balanced over a wide bandwidth.

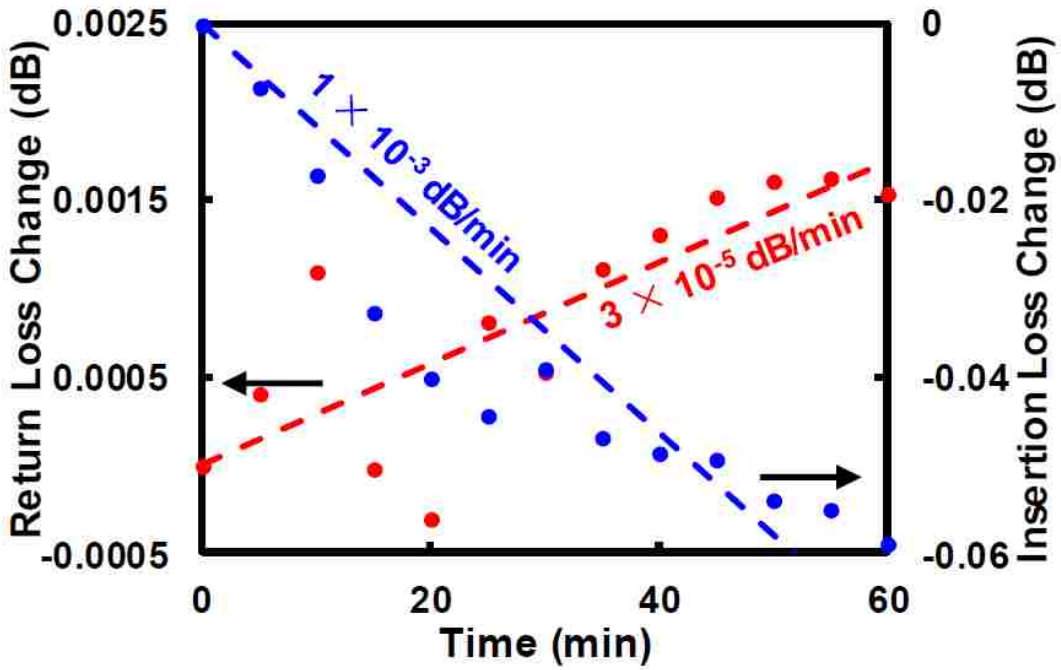

Fig. 17 Long-term drift of return and insertion losses at 9 GHz of a CPW with its series trap filled with sucrose solution

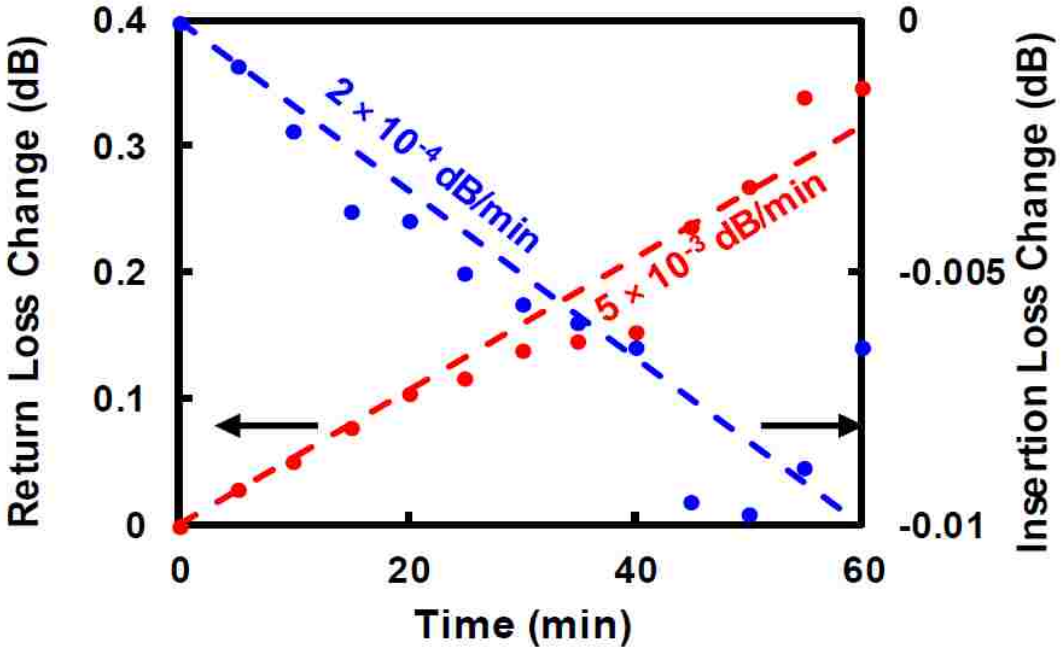

Fig. 18 Long-term drift of return and insertion losses at 9 GHz of a CPW with its shunt trap filled with sucrose solution

3.4 Summary

Single-cell characterization is the core part of the whole process, and has been studied for many years in our group. The progress introduced in the chapter is that now we are able to characterize the cell within an ultra-wideband covered from 9 kHz to 9 GHz, using keysight E5080A vector network analyzer with the help of an effective DEP trapping/detrapping. Single cell characterization experiments were accomplished in both series and shunt configurations with return loss change and insertion loss change shown in this chapter. Background drift was carefully studied to confirm the effective sensitivity of our charaterizations. Based on the S-parameters obtained, equivalent circuit model can be built for the cell and resistance and capacitance of the membrane and the cytoplasm will be extracted.

Chapter 4: Electroporation

4.1 Theory

Electroporation is commonly used to introduce polar or charged molecules into biological cells for drug treatment or genetic manipulation [22]. In most cases, short pulses from nanoseconds to milliseconds are applied to the cell to generate on its membrane nanometer-sized pores that heal readily afterward. However, due to the dispersion of the experimental setup, including that of cables, connectors and cell enclosures, the actual waveform or frequency content a cell experiences is often highly distorted [23]. Therefore, to study the dispersive effect and the fundamental mechanism of electroporation, continuous-wave (CW) sinusoidal signals of different frequencies should be applied in a linear setup. To this end, electroporation by CW signals in the kilohertz range has been reported [24]–[30]. In comparison, CW signals in the megahertz range have been much less studied since, at such high frequencies, a linear setup is more difficult to achieve [26] and the signals are thought to bypass mostly the cell membrane [27]. Thus, using a well-characterized linear setup [31], it is interesting to study electroporation under megahertz signals and to see whether or not they can be used for electroporation without affecting cell viability. In [31], using 10-MHz CW signals, we were successful for the first time in electroporation of Jurkat T-lymphoma human cells without causing cell death.

4.2 Experimental Results

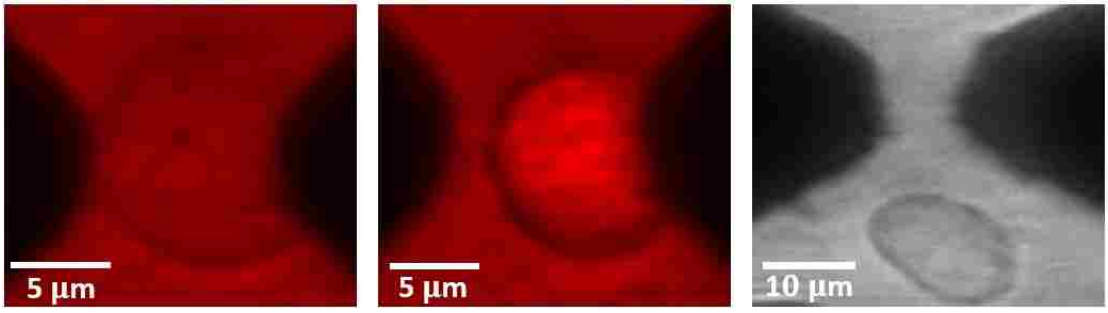

(a) (b) (c)

Fig. 19. Micrographs of a Jurkat cell (a) trapped, (b) porated, and (c) detrapped in series configuration, with poration confirmed by red dye of propidium iodide.

With a cell trapped, it can be electroporated by switching the VNA to 100 kHz and 9 dBm as listed in Table II. UWB characterization can then be conveniently performed before and after for correlation with changes in cell porosity, vitality and morphology, by using conventional fluorescent dyes [20], [32]. Finally, the cell can be de-trapped by switching the VNA to 10 kHz at 3 dBm, so the sequence of trapping, characterization, poration, and detrapping can be repeated on the next available cell. Fig. 19 shows the same cell trapped, porated and detrapped by the same VNA, with poration confirmed by propidium-iodide red-fluorescence dye.

4.3 Summary

Electroporation is a convenient technique to introduce polar or charged molecules into a biological cell for drug evaluation or genetic manipulation [1]. Under a pulsed or continuous-wave (CW) electrical signal, nanometer pores can form on the cell membrane to allow molecules

to diffuse in or out of the cell. The time it takes for poration varies as the effect of electrical stimulation is statistical and cumulative, and each cell is different biologically. In this chapter, electroporation has been accomplished by a network analyzer for the first time, with results demonstrated by the fluorescent dyes.

Chapter 5: Conclusions

For the first time, by conveniently programming the frequency and power of the same UWB VNA, single-cell trapping, characterization, poration, and de-trapping were demonstrated. This breakthrough not only greatly improves the accuracy and efficiency of UWB cell characterization, but also can enable its throughput to approach that of optical cytometers in the future. Single-cell detrapping experiments were used to validate the C-M function for predicting the crossover frequency from pDEP to nDEP. The validation was successful despite the highly nonuniform field distribution between small and closely spaced electrodes with the distribution greatly disturbed by the cell, with a good match with the calculated results. The C-M function can be used to refine the DEP con-figuration and algorithm for more complicated manipulation of single-cells. With ultra-wideband DEP trapping/detrapping, characterization, electroporation accomplished using the same network analyzer, a more integrated and programmable setup will be developed, bringing a bright expectation of a much higher throughput in the future.

References

[1] Kang, M.; Jung, S.; Zhang, H. N.; Kang, T.; Kang, H.; Yoo, Y.; Hong, J. P.; Ahn, J. P.; Kwak, J.; Jeon, D.; Kotov, N. A.; Kim, B., Subcellular Neural Probes from Single-Crystal Gold Nanowires. *ACS Nano* **2014,** *8* (8), 8182-8189.

[2] Xu, A. M.; Aalipour, A.; Leal-Ortiz, S.; Mekhdjian, A. H.; Xie, X.; Dunn, A. R.; Garner, C. C.; Melosh, N. A., Quantification of nanowire penetration into living cells. *Nature Communications* **2014,** *5*, 8.

[3] Zhang, G. J.; Huang, M. J.; Luo, Z. H. H.; Tay, G. K. I.; Lim, E. J. A.; Liu, E. T.; Thomsen, J. S., Highly sensitive and reversible silicon nanowire biosensor to study nuclear hormone receptor protein and response element DNA interactions. *Biosens. Bioelectron.* **2010,** *26* (2), 365-370.

[4] Ma, X.; Du, X.; N. Gholizadeh, V. G.; Li, H.; Cheng, X.; Hwang, J. C. M., One Resistor and Two Capacitors: An Electrical Engineer's Simple View of a Biological Cell. In *IEEE MTT-S International Microwave Workshop Series on Advanced Materials and Processes (IMWS-AMP 2017)*, IEEE, Ed. Pavia, Italy, 2017.

[5] Ma, X.; Du, X.; Multari, C. R.; Ning, Y.; Luo, X.; Gholizadeh, V.; Palego, C.; Cheng, X.; Hwang, J. C. M. In *Reproducible broadband measurement for cytoplasm capacitance of a biological cell*, 2016 IEEE MTT-S International Microwave Symposium (IMS), 22-27 May 2016; 2016; pp 1-4.

[6] V. F. Lvovich, *Impedance Spectroscopy: Applications to Electrochemical and Dielectric*

Phenomena. New York, NY, USA: John Wiley, 2012.

[7] V. Raicu and Y. Feldman, *Dielectric Relaxation in Biological Systems: Physical Principles, Methods, and Applications.* Oxford, UK: Oxford, 2015.

[8] T. Chen *et al.,* "Microwave biosensor dedicated to the dielectric spectroscopy of a single alive biological cell in its culture medium," in *IEEE MTT-S Int. Microwave Symp. (IMS) Dig.,* Jun. 2013, pp. 1–4.

[9] Y. Ning *et al.,* "Fast, compact and label-free electrical detection of live and dead single cells," in *Proc. IEEE MTT-S Int. Microwave Workshop Series RF Wireless Technologies Biomedical Healthcare Applications,* Singapore, Dec. 2013, pp. 1–3.

[10] Y. Ning *et al.,* "Broadband electrical detection of individual biological cells," *IEEE Trans. Microw. Theory Techn.,* vol. 62, no. 9, pp. 1905−1911, Sep. 2014.

[11] X. Du *et al.,* "Validation of Clausius-Mossotti function in single-cell dielectrophoresis," in *Proc. IEEE MTT-S Int. Microw. Biomed. Conf. (IMBioC),* Philadelphia, PA, USA, Jun. 2018, pp. 1−4.

[12] H. Li *et al.,* "Distributed effect in high-frequency electroporation of biological cells," *IEEE Trans. Microw. Theory Techn.,* vol. 65, no. 9, pp. 3503−3511, Sep. 2017.

[13] H. A. Pohl, *Dielectrophoresis: The Behavior of Neutral Matter in Nonuniform Electric Fields.* New York, NY, USA. Cambridge University Press, 1978.

[14] R. Pethig, *Dielectrophoresis: Theory, Methodology and Biological Applications.* New York, NY, USA. John Wiley & Sons, 2017.

[15] J. Oblak *et al.,* "Feasibility study for cell electroporation detection and separation by means of dielectrophoresis," *Bioelectrochemistry,* vol. 71, no. 2, pp. 164–171, Nov. 2007.

[16] Q. Hu, R. P. Joshi, and A. Beskok, "Model study of electroporation effects on the dielectrophoretic response of spheroidal cells," *J. Appl. Phys.,* vol. 106, no. 2, pp. 024701-1−024701-8, Jul. 2009.

[17] A. Denzi, F. Camera, C. Merla, B. Benassi, C. Consales, A. Paffi, F. Apollonio, and M. Liberti, "*A microdosimetric study of electropulsation on multiple realistically shaped cells: Effect of neighbours,*" *J. Membrane Biology*, vol. 249, no. 5, pp 691–701, Oct. 2016.

[18] E. Salimi *et al.,* "Dielectrophoresis study of temporal change in internal conductivity of single CHO cells after electroporation by pulsed electric fields," *Biomicrofluidics,* vol. 11, pp. 014111-1−014111-21, Feb. 2017

[19] X. Ma *et al.,* "Sensitivity analysis for broadband electro-magnetic characterization of biological cells," *IEEE Trans. Microw. Theory Techn.* Submitted for publication.

[20] H. Li *et al.,* "Correlation between morphology change and microwave property during single-cell electroporation," in *Dig. IEEE MTT-S Int. Microwave Symp. (IMS),* Honolulu, HI, Jun. 2017, pp. 1−3.

[21] X. Du *et al.,* "Ultra-wideband characterization, electroporation, and dielectrophoresis of a live biological cell using the same vector network analyzer," in *IEEE MTT-S Int. Microwave Symp. (IMS) Dig.,* Philadelphia, PA, USA, Jun. 2018, pp. 1−4.

[22] T. Kotnik, W. Frey, M. Sack, S. H. Meglic, M. Peterka, and D. Miklavcic, "Electroporation-

based applications in biotechnology," *Trends Biotechnol.,* vol. 33, no. 8, pp. 480–488, Aug. 2015.

[23] A. Denzi, C. Merla, C. Palego, F. Apollonio, J. C. M. Hwang, and M. Liberti, "Single cell microdosimetric studies comparing ideal and measured nanosecond pulsed electric fields," in *IEEE MTT-S Int. Microwave Symp. (IMS),* Seattle, WA, Jun. 2013, pp. 1–4.

[24] P. Marszalek, D. S. Liu, and T. Y. Tsong, "Schwan equation and transmembrane potential induced by alternating electric field," *Biophys. J.,* vol. 58, no. 4, pp. 1053–1058, Oct. 1990.

[25] E. Tekle, R. D. Astumian, and P. B. Chock, "Electroporation by using bipolar oscillating electric field: An improved method for DNA transfection of NIH 3T3 cells," *Proc. Natl. Acad. Sci. U. S. A.,* vol. 88, no. 10, pp. 4230–4234, May 1991.

[26] D. W. Jordan, R. M. Gilgenbach, M. D. Uhler, L. H. Gates, and Y. Y. Lau, "Effect of pulsed, high-power radiofrequency radiation on electroporation of mammalian cells," *IEEE Trans. Plasma Sci.,* vol. 32, no. 4, pp. 1573–1578, Aug. 2004.

[27] S. Katsuki, N. Nomura, H. Koga, H. Akiyama, I. Uchida, and S. I. Abe, "Biological effects of narrow band pulsed electric fields," *IEEE Trans. Dielectr. Electr. Insul.,* vol. 14, no. 3, pp. 663–668, Jun. 2007.

[28] C. Chen, J. A. Evans, M. P. Robinson, S. W. Smye, and P. O'Toole, "Measurement of the efficiency of cell membrane electroporation using pulsed ac fields," *Phys. Med. Biol.,* vol. 53, pp. 4747–4757, Aug. 2008.

[29] Y. Zhan, Z. Cao, N. Bao, J. Li, J. Wang, T. Geng, H. Lin, and C. Lu, "Low-frequency ac

electroporation shows strong frequency dependence and yields comparable transfection results to dc electroporation," *J. Controlled Release,* vol. 160, no. 3, pp. 570–576, Jun. 2012.

[30] T. Geng, Y. Zhan, and C. Lu, "Gene delivery by microfluidic flow-through electroporation based on constant DC and AC field," in *Proc. IEEE Eng. Med. Biol. Soc. Conf.,* San Diego, CA, Aug. 2012, pp. 2579–2582.

[31] H. Li, X. Ma, X. Du, X. Cheng, and J. C. M. Hwang, "High-frequency continuous-wave electroporation of Jurkat human lymphoma cells," in *IEEE MTT-S Int. Microwave Symp. (IMS),* San Francisco, CA, May 2016, pp. 1–4.

[32] H. Li *et al.,* "Correlation between optical fluorescence and microwave transmission during single-cell electroporation," *IEEE Trans. Biomed. Eng.* Submitted for publication.

Vita

Xiaotian Du received his B.S. degree in materials science from Fudan University, Shanghai, China in 2016. In 2014, He was an exchange student at UC Berkeley. Since July of 2015, he has been working as a research assistant in electrical engineering at Lehigh University, Bethlehem, Pennsylvania, USA. He is currently pursuing a Ph.D. degree in electrical engineering at Lehigh University. His research interest includes biosensors, micro-electromechanical systems, and other microwave devices and circuits.